Computer Physics Communications 180 (2009) 365–374

Contents lists available at ScienceDirect

Computer Physics Communications

www.elsevier.com/locate/cpc

Two-dimensional full-electromagnetic Vlasov code with conservative scheme and its application to magnetic reconnection

Takayuki Umeda *, Kentaro Togano, Tatsuki Ogino

Solar-Terrestrial Environment Laboratory, Nagoya University, Nagoya, Aichi 464-8601, Japan

ARTICLE INFO

Article history:
Received 3 June 2008
Received in revised form 16 September 2008
Accepted 2 November 2008
Available online 7 November 2008

PACS:
52.65.Ff
52.35.Vd
52.25.Dg
02.70.-c

Keywords:
Vlasov simulation
Conservative scheme
Magnetic reconnection

ABSTRACT

A detailed procedure of full-electromagnetic Vlasov simulation technique is presented. Our new unsplitting conservative scheme exactly satisfies the continuity equation for charge. The implicit Finite Difference Time Domain method is also adopted for computation of electromagnetic fields, which is not restricted by the CFL condition for light. The Geospace Environment Modeling magnetic reconnection challenge problem is adopted as a benchmark test. The characteristics of the present Vlasov code are studied by varying the resolution in configuration space.

1. Introduction

Computer simulations are now one of essential approaches in plasma physics. There are numerous types of self-consistent simulations that treat plasmas according to some approximations. This includes fluid codes using the magnetohydrodynamic (MHD) method, hall-MHD method, and multi-fluid method. The fluid codes are used to study global and macroscopic processes in space plasmas. Hybrid methods whereby treat ions as particles and electrons as a fluid to study mesoscopic or ion-scale processes. Nonlinear microscopic processes in space plasmas are studied with kinetic simulation codes. Numerical methods for kinetic simulations fall into two groups. One is particle-in-cell (PIC) method which follows motions of individual particles in a self-consistent electromagnetic field. Another approach is Vlasov method which follows spatial and temporal development of distribution functions in the position-velocity phase space.

In recent days MHD simulations are widely used for studies of global- and macro-scale phenomena. However, the MHD simulations need artificial resistivity, conductivity, adiabatic index, and diffusion coefficients. These quantities are essentially due to kinetic processes that are eliminated by the MHD approximation. Although full-kinetic global simulation will be a final goal of computational plasma physics, this requires an enormous computing resource. There are recent attempts to directly simulate global- and macro-scale processes via full-kinetic codes. A typical example is the magnetic reconnection.

Recently full-kinetic simulations of magnetic reconnection were performed with several types of PIC codes in the framework of Geospace Environment Modeling (GEM) magnetic reconnection challenge [1]. The full-electromagnetic PIC code, in which both electrons and ions are treated as particles, is very useful for describing the full kinetics of plasmas. Especially, the explicit PIC method is a well-developed numerical technique which has benefits that numerical procedures and concepts are quite simple without approximation in the basic laws of collisionless plasmas. However, this method has two severe restrictions.

The first restriction is grid spacing (cell size). We need to set the grid spacing Δx to be as small as the electron Debye length. When the grid spacing is much larger than the electron Debye length, thermal noises of plasma particles are numerically enhanced by a nonphysical instability caused by the grid. Thus it is still difficult to perform large PIC simulations of MHD-scale processes due to the

* Corresponding author.
E-mail address: umeda@stelab.nagoya-u.ac.jp (T. Umeda).

0010-4655/$ – see front matter
doi:10.1016/j.cpc.2008.11.001

limitation of computer resources. The implicit PIC methods can relax the constraint. A fully implicit time stepping PIC method was used for GEM magnetic reconnection challenge [2]. However, the numerical procedures are much more complicated than those of the explicit PIC method. An alternative is the use of adaptive mesh refinement technique [3], the numerical procedures of which are also complicated. The Vlasov method might be another alternative to the PIC method, because the Vlasov method is free from any numerical noise. Owing to the rapid development of supercomputer technology, the Vlasov method is rapidly developing. However, there are few benchmark tests of the Vlasov method which treats global- and macro-scale processes. It is not clear whether the Vlasov method can relax the constraint of grid spacing.

The second restriction is the CFL condition for light. That is, the time step Δt has to be chosen such that the speed of light c is resolved on the numerical grid. That is, we need to set the grid spacing to be $\Delta x > c\Delta t$. One way to avoid this is to use the Darwin approximation in which electromagnetic vacuum (light) modes are suppressed by neglecting the displacement current due to the transverse electric fields. In the framework of the Darwin approximation, low-frequency electrostatic, magnetostatic, and inductive fields are considered. The Darwin approximation has been widely used in the PIC method (e.g., Ref. [4]). Recently a Darwin–Vlasov code was developed by Schmitz and Grauer [5] and was successfully used for GEM magnetic reconnection challenge [6]. An alternative method to avoid the CFL condition for light is the use of an implicit Finite Difference Time Domain (FDTD) method for solving Maxwell's equations.

The purpose of the present study is to give simple and efficient numerical techniques for full-electromagnetic Vlasov method. In this paper, we present an unsplitting conservative scheme which exactly satisfies the charge conservation. We also adopted the implicit FDTD method which is not restricted by the CFL condition for light. Another purpose is to study restriction of grid spacing in the Vlasov method by using grid spacings much larger than the electron Debye length. In order to benchmark the full-electromagnetic Vlasov method, the Geospace Environment Modeling (GEM) magnetic reconnection challenge problem is adopted.

This paper is structured as follows. In Section 2, we present the detailed numerical procedure for full-electromagnetic Vlasov method. A new unsplitting conservative scheme and the implicit FDTD method are introduced. In Section 3, we describe simulation setup of the GEM reconnection challenge and detailed simulation parameters. Simulation results are presented in Section 4, and summary of this paper is given in Section 5.

2. Methods

2.1. Basic equations and timestep chart

The present full-electromagnetic Vlasov code solves the full-set of Maxwell's equations (1) and the Vlasov equation (2),

$$\nabla \times \boldsymbol{B} = \mu_0 \boldsymbol{J} + \frac{1}{c^2}\frac{\partial \boldsymbol{E}}{\partial t},$$
$$\nabla \times \boldsymbol{E} = -\frac{\partial \boldsymbol{B}}{\partial t},$$
$$\nabla \cdot \boldsymbol{E} = \frac{\rho}{\epsilon_0},$$
$$\nabla \cdot \boldsymbol{B} = 0, \tag{1}$$
$$\frac{\partial f_s}{\partial t} + \boldsymbol{v}\frac{\partial f_s}{\partial \boldsymbol{x}} + \frac{q_s}{m_s}[\boldsymbol{E} + \boldsymbol{v} \times \boldsymbol{B}]\frac{\partial f_s}{\partial \boldsymbol{v}} = 0, \tag{2}$$

where $\boldsymbol{E}$, $\boldsymbol{B}$, $\boldsymbol{J}$, ρ, μ_0, ϵ_0 and c represent electric field, magnetic field, current density, charge density, magnetic permeability, dielectric constant and light speed, respectively. Here $f_s(\boldsymbol{x}, \boldsymbol{v}, t)$ is the distribution function of species s in a position-velocity phase space. In this paper, only singly-charged ions and electrons ($s = i, e$) are considered, although the code allows arbitrary species. The quantities q_s and m_s are the charge and mass of particle species s. The current density $\boldsymbol{J}$ is determined so that ρ and $\boldsymbol{J}$ satisfy the continuity equation for charge

$$\frac{\partial \rho}{\partial t} + \nabla \cdot \boldsymbol{J} = 0. \tag{3}$$

For stable time-integration of the Vlasov equation, we use a modified splitting scheme which is an extension of the original splitting scheme [7,8]. The Vlasov equation splits into the following three advection equations (e.g., Ref. [9]),

$$\frac{\partial f_s}{\partial t} + \boldsymbol{v}\frac{\partial f_s}{\partial \boldsymbol{x}} = 0, \tag{4}$$
$$\frac{\partial f_s}{\partial t} + \frac{q_s}{m_s}\boldsymbol{E}\frac{\partial f_s}{\partial \boldsymbol{v}} = 0, \tag{5}$$
$$\frac{\partial f_s}{\partial t} + \frac{q_s}{m_s}[\boldsymbol{v} \times \boldsymbol{B}]\frac{\partial f_s}{\partial \boldsymbol{v}} = 0. \tag{6}$$

Eqs. (4) and (5) are scalar (linear) advection equations in which $\boldsymbol{v}$ and $\boldsymbol{E}$ are independent of $\boldsymbol{x}$ and $\boldsymbol{v}$, respectively. Thus semi-Lagrangian schemes are straightforwardly applied. Eq. (6), on the other hand, is a multi-dimensional rotation equation which follows a circular motion of a profile at constant speed by a centripetal force. For stable rotation of distribution functions on the Cartesian grid system, we adopt the "back-substitution" scheme developed by Schmitz and Grauer [10].

In the present study, we consider two-dimensional configuration and three-dimensional velocity spaces which is so-called the two-and-half-dimensional system. The full Maxwell–Vlasov system is advanced by using the following sequences,

(1) Shift phase-space distribution functions in the configuration space with the full time step Δt (see Section 2.2).

$$f_s^*(x, y, v_x, v_y, v_z) = f_s^t(x - v_x\Delta t, y - v_y\Delta t, v_x, v_y, v_z). \tag{7}$$

(2) Compute the current density (see Section 2.2).
(3) Advance electromagnetic fields by solving Maxwell's equations with the full time step Δt (see Section 2.3).
(4) Shift phase-space distribution functions in the velocity space by an electric force with the half time step $\Delta t/2$ (see Section 2.2).

$$f_s^{**}(x, y, v_x, v_y, v_z) = f_s^{*}\left(x, y, v_x - \frac{q_s}{m_s}E_x^{t+\Delta t}\Delta t, v_y - \frac{q_s}{m_s}E_y^{t+\Delta t}\Delta t, v_z - \frac{q_s}{m_s}E_z^{t+\Delta t}\Delta t\right). \tag{8}$$

(5) Rotate phase-space distribution functions in the velocity space by a magnetic force with the full time step Δt by using the back-substitution scheme [10].

$$f_s^{***}(x, y, v_x, v_y, v_z) = f_s^{**}\left(x, y, v_x^*, v_y^*, v_z^*\right), \tag{9}$$

where

$$\boldsymbol{v}^* = \boldsymbol{v} - \frac{q_s}{m_s}\frac{\Delta t}{1+\left[\frac{q_s}{m_s}\frac{\Delta t}{2}|\boldsymbol{B}^{t+\Delta t}|\right]^2}\left[\boldsymbol{v}\times\boldsymbol{B}^{t+\Delta t}\right] + \frac{q_s^2}{m_s^2}\frac{\Delta t^2}{2+2\left[\frac{q_s}{m_s}\frac{\Delta t}{2}|\boldsymbol{B}^{t+\Delta t}|\right]^2}\left[\boldsymbol{v}\times\boldsymbol{B}^{t+\Delta t}\times\boldsymbol{B}^{t+\Delta t}\right]. \tag{10}$$

(6) Shift phase-space distribution functions in the velocity space by an electric force with the half time step $\Delta t/2$ (see Section 2.2).

$$f_s^{t+\Delta t}(x, y, v_x, v_y, v_z) = f_s^{***}\left(x, y, v_x - \frac{q_s}{m_s}E_x^{t+\Delta t}\Delta t, v_y - \frac{q_s}{m_s}E_y^{t+\Delta t}\Delta t, v_z - \frac{q_s}{m_s}E_z^{t+\Delta t}\Delta t\right). \tag{11}$$

It should be noted that the timestep chart listed above is equivalent to the timestep chart of standard PIC methods, which is so-called 2nd-order leap-frog time-integration.

2.2. Unsplitting conservative scheme

Let us consider that a numerical solution to Eq. (7) takes the following conservative form,

$$\begin{aligned} f_s^{*}(x_i, y_j, v_{x,l}, v_{y,m}, v_{z,n}) = {} & f_s^{t}(x_i, y_j, v_{x,l}, v_{y,m}, v_{z,n}) \\ & - \frac{\Delta t}{\Delta x}\left[U_{x,s}\left(x_{i+\frac{1}{2}}, y_j, v_{x,l}, v_{y,m}, v_{z,n}\right) - U_{x,s}\left(x_{i-\frac{1}{2}}, y_j, v_{x,l}, v_{y,m}, v_{z,n}\right)\right] \\ & - \frac{\Delta t}{\Delta y}\left[U_{y,s}\left(x_i, y_{j+\frac{1}{2}}, v_{x,l}, v_{y,m}, v_{z,n}\right) - U_{y,s}\left(x_i, y_{j-\frac{1}{2}}, v_{x,l}, v_{y,m}, v_{z,n}\right)\right] \end{aligned} \tag{12}$$

where U_x and U_y are numerical fluxes in the x and y directions, respectively. In the present study, we use an unsplitting scheme (e.g., [11]) instead of the conventional directional splitting scheme.

Let us consider transportation of a conserved quantity as schematically illustrated in Fig. 1. With the directional splitting scheme, the conserved quantity is integrated in time by transportation along the system axes in the alternative order,

$$\begin{aligned} f^{*}(x_i, y_j) &= f^{t}(x_i, y_j) - \frac{\Delta t}{2\Delta x}\left[U_x^{t,1\mathrm{D}}\left(x_{i+\frac{1}{2}}, y_j\right) - U_x^{t,1\mathrm{D}}\left(x_{i-\frac{1}{2}}, y_j\right)\right], \\ f^{**}(x_i, y_j) &= f^{*}(x_i, y_j) - \frac{\Delta t}{2\Delta x}\left[U_y^{*,1\mathrm{D}}\left(x_i, y_{j+\frac{1}{2}}\right) - U_y^{*,1\mathrm{D}}\left(x_i, y_{j-\frac{1}{2}}\right)\right], \\ f^{***}(x_i, y_j) &= f^{**}(x_i, y_j) - \frac{\Delta t}{2\Delta x}\left[U_y^{**,1\mathrm{D}}\left(x_i, y_{j+\frac{1}{2}}\right) - U_y^{**,1\mathrm{D}}\left(x_i, y_{j-\frac{1}{2}}\right)\right], \\ f^{t+\Delta t}(x_i, y_j) &= f^{***}(x_i, y_j) - \frac{\Delta t}{2\Delta x}\left[U_x^{***,1\mathrm{D}}\left(x_{i+\frac{1}{2}}, y_j\right) - U_x^{***,1\mathrm{D}}\left(x_{i-\frac{1}{2}}, y_j\right)\right]. \end{aligned} \tag{13}$$

The one-dimensional numerical flux $U^{1\mathrm{D}}$ is computed by using an arbitrary conservative scheme. With the 1st-order upwind scheme, for example, the one-dimensional numerical flux is given as

$$U_x^{\tau,1\mathrm{D}}\left(x_{i+\frac{1}{2}}, y_j\right) = \begin{cases} v_x f^{\tau}(x_i, y_j) & \text{for } v_x \geqslant 0, \\ v_x f^{\tau}(x_{i+1}, y_j) & \text{for } v_x < 0, \end{cases} \tag{14}$$

$$U_y^{\tau,1\mathrm{D}}\left(x_i, y_{j+\frac{1}{2}}\right) = \begin{cases} v_y f^{\tau}(x_i, y_j) & \text{for } v_y \geqslant 0, \\ v_y f^{\tau}(x_i, y_{j+1}) & \text{for } v_y < 0. \end{cases} \tag{15}$$

Then, the new profile of the conserved quantity at $t+\Delta t$ in Fig. 1 ($v_x > 0$ and $v_y < 0$) becomes

$$\begin{aligned} f^{t+\Delta t}(x_i, y_j) &= \left[1 - v_x\frac{\Delta t}{\Delta x}\right]\left[1 - v_y\frac{\Delta t}{\Delta y}\right]f^{t}(x_i, y_j), \\ f^{t+\Delta t}(x_{i+1}, y_j) &= \left[v_x\frac{\Delta t}{\Delta x}\right]\left[1 - v_y\frac{\Delta t}{\Delta y}\right]f^{t}(x_i, y_j), \\ f^{t+\Delta t}(x_i, y_{j-1}) &= \left[1 - v_x\frac{\Delta t}{\Delta x}\right]\left[v_y\frac{\Delta t}{\Delta y}\right]f^{t}(x_i, y_j), \\ f^{t+\Delta t}(x_{i+1}, y_{j-1}) &= \left[v_x\frac{\Delta t}{\Delta x}\right]\left[v_y\frac{\Delta t}{\Delta y}\right]f^{t}(x_i, y_j). \end{aligned} \tag{16}$$

Let us extend Eq. (13) to an unsplitting scheme,

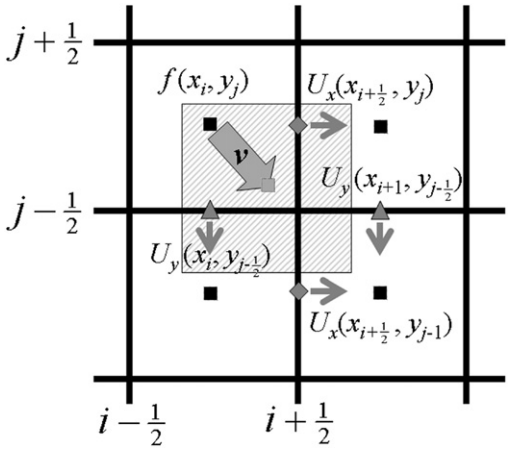

Fig. 1. Transportation of a conserved quantity f in two dimension.

$$f^{t+\Delta t}(x_i, y_j) = f^t(x_i, y_j) - \frac{\Delta t}{\Delta x}\left[U_x\left(x_{i+\frac{1}{2}}, y_j\right) - U_x\left(x_{i-\frac{1}{2}}, y_j\right)\right] - \frac{\Delta t}{\Delta y}\left[U_y\left(x_i, y_{j+\frac{1}{2}}\right) - U_y\left(x_i, y_{j-\frac{1}{2}}\right)\right]. \tag{17}$$

From Fig. 1, we can assume the following boundary conditions, $U_x(x_{i-\frac{1}{2}}, y_{j-1}) = 0$, $U_x(x_{i+\frac{3}{2}}, y_{j-1}) = 0$, $U_x(x_{i-\frac{1}{2}}, y_j) = 0$, $U_x(x_{i+\frac{3}{2}}, y_j) = 0$, $U_y(x_i, y_{j+\frac{1}{2}}) = 0$, $U_y(x_i, y_{j-\frac{3}{2}}) = 0$, $U_y(x_{i+1}, y_{j+\frac{1}{2}}) = 0$, and $U_y(x_{i+1}, y_{j-\frac{3}{2}}) = 0$. Then we obtain the following continuity equations,

$$\begin{aligned}
f^{t+\Delta t}(x_i, y_j) &= f^t(x_i, y_j) - \frac{\Delta t}{\Delta x}U_x\left(x_{i+\frac{1}{2}}, y_j\right) + \frac{\Delta t}{\Delta y}U_y\left(x_i, y_{j-\frac{1}{2}}\right),\\
f^{t+\Delta t}(x_{i+1}, y_j) &= f^t(x_{i+1}, y_j) + \frac{\Delta t}{\Delta x}U_x\left(x_{i+\frac{1}{2}}, y_j\right) + \frac{\Delta t}{\Delta y}U_y\left(x_{i+1}, y_{j-\frac{1}{2}}\right),\\
f^{t+\Delta t}(x_i, y_{j-1}) &= f^t(x_i, y_{j-1}) - \frac{\Delta t}{\Delta x}U_x\left(x_{i+\frac{1}{2}}, y_{j-1}\right) - \frac{\Delta t}{\Delta y}U_y\left(x_i, y_{j-\frac{1}{2}}\right),\\
f^{t+\Delta t}(x_{i+1}, y_{j-1}) &= f^t(x_{i+1}, y_{j-1}) + \frac{\Delta t}{\Delta x}U_x\left(x_{i+\frac{1}{2}}, y_{j-1}\right) - \frac{\Delta t}{\Delta y}U_y\left(x_{i+1}, y_{j-\frac{1}{2}}\right).
\end{aligned} \tag{18}$$

From Eq. (16), we obtain the following three equations,

$$\begin{aligned}
&U_x\left(x_{i+\frac{1}{2}}, y_{j-1}\right) + U_x\left(x_{i+\frac{1}{2}}, y_j\right) = v_x f^t(x_i, y_j),\\
&U_y\left(x_i, y_{j-\frac{1}{2}}\right) + U_y\left(x_{i+1}, y_{j-\frac{1}{2}}\right) = v_y f^t(x_i, y_j),\\
&\frac{\Delta t}{\Delta x}U_x\left(x_{i+\frac{1}{2}}, y_{j-1}\right) - \frac{\Delta t}{\Delta y}U_y\left(x_{i+1}, y_{j-\frac{1}{2}}\right) = \left[v_x\frac{\Delta t}{\Delta x}\right]\left[v_y\frac{\Delta t}{\Delta y}\right]f^t(x_i, y_j).
\end{aligned} \tag{19}$$

There is an arbitrary solution to the above equations because there are 4 variables while there is only 3 equations. In order to simplify the computation, we assume that

$$\frac{\Delta t}{\Delta x}U_x\left(x_{i+\frac{1}{2}}, y_{j-1}\right) = -\frac{\Delta t}{\Delta y}U_y\left(x_{i+1}, y_{j-\frac{1}{2}}\right). \tag{20}$$

Thus the two-dimensional numerical flux is given as

$$\begin{aligned}
U_x\left(x_{i+\frac{1}{2}}, y_j\right) &= v_x f^t(x_i, y_j) - \left[\frac{v_x v_y}{2}\frac{\Delta t}{\Delta y}\right]f^t(x_i, y_j),\\
U_x\left(x_{i+\frac{1}{2}}, y_{j-1}\right) &= \left[\frac{v_x v_y}{2}\frac{\Delta t}{\Delta y}\right]f^t(x_i, y_j),\\
U_y\left(x_i, y_{j-\frac{1}{2}}\right) &= v_y f^t(x_i, y_j) + \left[\frac{v_x v_y}{2}\frac{\Delta t}{\Delta x}\right]f^t(x_i, y_j),\\
U_y\left(x_{i+1}, y_{j-\frac{1}{2}}\right) &= -\left[\frac{v_x v_y}{2}\frac{\Delta t}{\Delta x}\right]f^t(x_i, y_j).
\end{aligned} \tag{21}$$

Taking into account the direction of flux, two-dimensional numerical flux with an arbitrary one-dimensional conservative scheme can be approximated as follows,

$$U_{x,s}\left(x_{i+\frac{\sigma_i}{2}}, y_j\right) = U^{1D}_{x,s}\left(x_{i+\frac{\sigma_i}{2}}, y_j\right)\left[1 - \sigma_i \frac{\Delta t}{\Delta y}\frac{U^{1D}_{y,s}(x_i, y_{j+\frac{\sigma_j}{2}})}{2 f^t_s(x_i, y_j)}\right],$$

$$U_{x,s}\left(x_{i+\frac{\sigma_i}{2}}, y_{j+\sigma_j}\right) = \sigma_i \frac{\Delta t}{\Delta y}\frac{U^{1D}_{x,s}(x_{i+\frac{\sigma_i}{2}}, y_j) U^{1D}_{y,s}(x_i, y_{j+\frac{\sigma_j}{2}})}{2 f^t_s(x_i, y_j)},$$

$$U_{y,s}\left(x_i, y_{j+\frac{\sigma_j}{2}}\right) = U^{1D}_{y,s}\left(x_i, y_{j+\frac{\sigma_j}{2}}\right)\left[1 - \sigma_j \frac{\Delta t}{\Delta x}\frac{U^{1D}_{x,s}(x_i, y_{j+\frac{\sigma_j}{2}})}{2 f^t_s(x_i, y_j)}\right],$$

$$U_{y,s}\left(x_{i+\sigma_i}, y_{j+\frac{\sigma_j}{2}}\right) = \sigma_j \frac{\Delta t}{\Delta x}\frac{U^{1D}_{x,s}(x_{i+\frac{\sigma_i}{2}}, y_j) U^{1D}_{y,s}(x_i, y_{j+\frac{\sigma_j}{2}})}{2 f^t_s(x_i, y_j)}, \tag{22}$$

where $\sigma_i = \mathrm{sign}(v_{x,l})$ and $\sigma_j = \mathrm{sign}(v_{y,m})$. Note that $v_{x,l}$, $v_{y,m}$, and $v_{z,n}$ are omitted for simplicity. There is an arbitrary solution for the multi-dimensional numerical flux. In order to simplify computation, we assume Eq. (20) and approximate the two-dimensional numerical flux as follows:

$$\sigma_i \frac{\Delta t}{\Delta x} U_{x,s}\left(x_{i+\frac{\sigma_i}{2}}, y_{j+\sigma_j}\right) = \sigma_j \frac{\Delta t}{\Delta y} U_{y,s}\left(x_{i+\sigma_i}, y_{j+\frac{\sigma_j}{2}}\right), \tag{23}$$

$$\sim \frac{\Delta t^2}{\Delta x \Delta y}\frac{U^{1D}_{x,s}(x_{i+\frac{\sigma_i}{2}}, y_j) U^{1D}_{y,s}(x_i, y_{j+\frac{\sigma_j}{2}})}{2 f^t_s(x_i, y_j)} + \mathcal{O}(\Delta x \Delta y). \tag{24}$$

It should be noted that we can compute the two-dimensional numerical flux as a function of both v_x and v_y instead of the simple multiplication of U^{1D}_x and U^{1D}_y. However, we found that there was not critical difference between the computational results. Hence we have adopted the simple approximation.

In the present study a positive, non-oscillatory and conservative scheme with cubic polynomials [12] is adopted to compute one-dimensional numerical flux U^{1D}. Since detailed descriptions on the conservative scheme is presented in Refs. [12–14], these are not repeated here.

Let us take the sum of Eq. (12) over the velocity grids. The charge density is given by

$$\rho^t(x_i, y_j) = \sum_s q_s \sum_l \sum_m \sum_n f^t_s(x_i, y_j, v_{x,l}, v_{y,m}, v_{z,n}) \Delta v_x \Delta v_y \Delta v_z. \tag{25}$$

In the present study, we compute the current density by

$$J^{t+\frac{\Delta t}{t}}_x\left(x_{i+\frac{1}{2}}, y_j\right) = \sum_s q_s \sum_l \sum_m \sum_n U_{x,s}\left(x_{i+\frac{1}{2}}, y_j, v_{x,l}, v_{y,m}, v_{z,n}\right) \Delta v_x \Delta v_y \Delta v_z,$$

$$J^{t+\frac{\Delta t}{t}}_y\left(x_i, y_{j+\frac{1}{2}}\right) = \sum_s q_s \sum_l \sum_m \sum_n U_{y,s}\left(x_i, y_{j+\frac{1}{2}}, v_{x,l}, v_{y,m}, v_{z,n}\right) \Delta v_x \Delta v_y \Delta v_z. \tag{26}$$

Then we obtain the difference form of the continuity equation for charge,

$$\frac{\rho^*(x_i, y_j) - \rho^t(x_i, y_j)}{\Delta t} = -\frac{J^{t+\frac{\Delta t}{t}}_x(x_{i+\frac{1}{2}}, y_j) - J^{t+\frac{\Delta t}{t}}_x(x_{i-\frac{1}{2}}, y_j)}{\Delta x} - \frac{J^{t+\frac{\Delta t}{t}}_y(x_i, y_{j+\frac{1}{2}}) - J^{t+\frac{\Delta t}{t}}_y(x_i, y_{j-\frac{1}{2}})}{\Delta y}. \tag{27}$$

Here $\rho^* = \rho^{t+\Delta t}$ because there is no advection in configuration space in (iv)–(vi). This implies that the continuity equation for charge is *exactly* satisfied in the present scheme. For the out-of-plane current density J_z, which is free from the charge conservation law, we take the sum of charge flux,

$$J^{t+\frac{\Delta t}{t}}_z(x_i, y_j) = \sum_s q_s \sum_l \sum_m \sum_n v_{z,n} \frac{f^*_s + f^t_s}{2}(x_i, y_j, v_{x,l}, v_{y,m}, v_{z,n}) \Delta v_x \Delta v_y \Delta v_z. \tag{28}$$

In a similar way, we use the unsplitting conservative scheme for Eqs. (8) and (11).

$$\begin{aligned} f''_s(x_i, y_j, v_{x,l}, v_{y,m}, v_{z,n}) = {} & f'_s(x_i, y_j, v_{x,l}, v_{y,m}, v_{z,n}) \\ & - \frac{\Delta t}{\Delta v_x}\left[W_{x,s}\left(x_i, y_j, v_{x,l+\frac{1}{2}}, v_{y,m}, v_{z,n}\right) - W_{x,s}\left(x_i, y_j, v_{x,l-\frac{1}{2}}, v_{y,m}, v_{z,n}\right)\right] \\ & - \frac{\Delta t}{\Delta v_y}\left[W_{y,s}\left(x_i, y_j, v_{x,l}, v_{y,m+\frac{1}{2}}, v_{z,n}\right) - W_{y,s}\left(x_i, y_j, v_{x,l}, v_{y,m-\frac{1}{2}}, v_{z,n}\right)\right] \\ & - \frac{\Delta t}{\Delta v_z}\left[W_{z,s}\left(x_i, y_j, v_{x,l}, v_{y,m}, v_{z,n+\frac{1}{2}}\right) - W_{z,s}\left(x_i, y_j, v_{x,l}, v_{y,m}, v_{z,n-\frac{1}{2}}\right)\right]. \end{aligned} \tag{29}$$

The three-dimensional numerical fluxes are approximated with the one-dimensional numerical fluxes as follows,

$$W_{x,s}\left(v_{x,l+\frac{\sigma_l}{2}}, v_{y,m}, v_{z,n}\right) = W^{1D}_{x,s}\left(v_{x,l+\frac{\sigma_l}{2}}, v_{y,m}, v_{z,n}\right) - \sigma_l\left[\frac{\Delta t}{\Delta y} W''_{xy,s} + \frac{\Delta t}{\Delta z} W''_{zx,s} - \frac{\Delta t^2}{\Delta y \Delta z} W'''_{xyz,s}\right],$$

$$W_{x,s}\left(v_{x,l+\frac{\sigma_l}{2}}, v_{y,m+\sigma_m}, v_{z,n}\right) = \sigma_l\left[\frac{\Delta t}{\Delta y} W''_{xy,s} - \frac{\Delta t^2}{\Delta y \Delta z} W'''_{xyz,s}\right],$$

$$
\begin{aligned}
&W_{x,s}\left(v_{x,l+\frac{\sigma_l}{2}}, v_{y,m}, v_{z,n+\sigma_n}\right) = \sigma_l\left[\frac{\Delta t}{\Delta z}W''_{zx,s} - \frac{\Delta t^2}{\Delta y \Delta z}W'''_{xyz,s}\right],\\
&W_{x,s}\left(v_{x,l+\frac{\sigma_l}{2}}, v_{y,m+\sigma_m}, v_{z,n+\sigma_n}\right) = \sigma_l\frac{\Delta t^2}{\Delta y \Delta z}W'''_{xyz,s},\\
&W_{y,s}\left(v_{x,l}, v_{y,m+\frac{\sigma_m}{2}}, v_{z,n}\right) = W^{1D}_{y,s}\left(v_{x,l}, v_{y,m+\frac{\sigma_m}{2}}, v_{z,n}\right) - \sigma_m\left[\frac{\Delta t}{\Delta x}W''_{xy,s} + \frac{\Delta t}{\Delta z}W''_{yz,s} - \frac{\Delta t^2}{\Delta x \Delta z}W'''_{xyz,s}\right],\\
&W_{y,s}\left(v_{x,l+\sigma_l}, v_{y,m+\frac{\sigma_m}{2}}, v_{z,n}\right) = \sigma_m\left[\frac{\Delta t}{\Delta x}W''_{xy,s} - \frac{\Delta t^2}{\Delta x \Delta z}W'''_{xyz,s}\right],\\
&W_{y,s}\left(v_{x,l}, v_{y,m+\frac{\sigma_m}{2}}, v_{z,n+\sigma_n}\right) = \sigma_m\left[\frac{\Delta t}{\Delta z}W''_{yz,s} - \frac{\Delta t^2}{\Delta x \Delta z}W'''_{xyz,s}\right],\\
&W_{y,s}\left(v_{x,l+\sigma_l}, v_{y,m+\frac{\sigma_m}{2}}, v_{z,n+\sigma_n}\right) = \sigma_m\frac{\Delta t^2}{\Delta x \Delta z}W'''_{xyz,s},\\
&W_{z,s}\left(v_{x,l}, v_{y,m}, v_{z,n+\frac{\sigma_n}{2}}\right) = W^{1D}_{z,s}\left(v_{x,l}, v_{y,m}, v_{z,n+\frac{\sigma_n}{2}}\right) - \sigma_n\left[\frac{\Delta t}{\Delta y}W''_{yz,s} + \frac{\Delta t}{\Delta x}W''_{zx,s} - \frac{\Delta t^2}{\Delta y \Delta z}W'''_{xyz,s}\right],\\
&W_{z,s}\left(v_{x,l+\sigma_l}, v_{y,m}, v_{z,n+\frac{\sigma_n}{2}}\right) = \sigma_n\left[\frac{\Delta t}{\Delta x}W''_{zx,s} - \frac{\Delta t^2}{\Delta y \Delta z}W'''_{xyz,s}\right],\\
&W_{z,s}\left(v_{x,l}, v_{y,m+\sigma_m}, v_{z,n+\frac{\sigma_n}{2}}\right) = \sigma_n\left[\frac{\Delta t}{\Delta y}W''_{yz,s} - \frac{\Delta t^2}{\Delta y \Delta z}W'''_{xyz,s}\right],\\
&W_{z,s}\left(v_{x,l+\sigma_l}, v_{y,m+\sigma_m}, v_{z,n+\frac{\sigma_n}{2}}\right) = \sigma_n\frac{\Delta t^2}{\Delta y \Delta z}W'''_{xyz,s},
\end{aligned}
\tag{30}
$$

where

$$
\begin{aligned}
W''_{xy,s} &= \frac{W^{1D}_{x,s}(v_{x,l+\frac{\sigma_l}{2}}, v_{y,m}, v_{z,n})W^{1D}_{y,s}(v_{x,l}, v_{y,m+\frac{\sigma_m}{2}}, v_{z,n})}{2f'_s(v_{x,l}, v_{y,m}, v_{z,n})},\\
W''_{yz,s} &= \frac{W^{1D}_{y,s}(v_{x,l}, v_{y,m+\frac{\sigma_m}{2}}, v_{z,n})W^{1D}_{z,s}(v_{x,l}, v_{y,m}, v_{z,n+\frac{\sigma_n}{2}})}{2f'_s(v_{x,l}, v_{y,m}, v_{z,n})},\\
W''_{zx,s} &= \frac{W^{1D}_{z,s}(v_{x,l}, v_{y,m}, v_{z,n+\frac{\sigma_n}{2}})W^{1D}_{x,s}(v_{x,l+\frac{\sigma_l}{2}}, v_{y,m}, v_{z,n})}{2f'_s(v_{x,l}, v_{y,m}, v_{z,n})},\\
W'''_{xyz,s} &= \frac{W^{1D}_{x,s}(v_{x,l+\frac{\sigma_l}{2}}, v_{y,m}, v_{z,n})W^{1D}_{y,s}(v_{x,l}, v_{y,m+\frac{\sigma_m}{2}}, v_{z,n})W^{1D}_{z,s}(v_{x,l}, v_{y,m}, v_{z,n+\frac{\sigma_n}{2}})}{3[f'_s(v_{x,l}, v_{y,m}, v_{z,n})]^2}
\end{aligned}
\tag{31}
$$

and $\sigma_l = \mathrm{sign}(\frac{q_s}{m_s}E_x(x_i, y_j))$, $\sigma_m = \mathrm{sign}(\frac{q_s}{m_s}E_y(x_i, y_j))$, and $\sigma_n = \mathrm{sign}(\frac{q_s}{m_s}E_z(x_i, y_j))$. Note that x_i and y_j are omitted for simplicity.

It should be noted that the unsplitting conservative scheme in its present form is restricted by the CFL condition. Extension to a CFL-free scheme is left as a future work.

2.3. Implicit FDTD method

We use an implicit FDTD method. Electromagnetic fields are discretized in space with the Yee grid system [15], while they are discretized in time as follows,

$$
\frac{\boldsymbol{E}^{t+\Delta t} - \boldsymbol{E}^t}{\Delta t} = -\frac{1}{\epsilon_0}\boldsymbol{J}^{t+\frac{\Delta t}{2}} + c^2\left[(1-\tau)\nabla\times\boldsymbol{B}^t + \tau\nabla\times\boldsymbol{B}^{t+\Delta t}\right], \tag{32}
$$

$$
\frac{\boldsymbol{B}^{t+\Delta t} - \boldsymbol{B}^t}{\Delta t} = -\left[(1-\tau)\nabla\times\boldsymbol{E}^t + \tau\nabla\times\boldsymbol{E}^{t+\Delta t}\right]. \tag{33}
$$

With an implicit factor $0.5 \leqslant \tau \leqslant 1.0$, the time-integration of electromagnetic fields is not restricted by the CFL condition of light.

Inserting Eq. (32) into Eq. (33), we obtain

$$
\left[1 - \tau^2 c^2 \Delta t^2 \nabla^2\right]\left[\frac{\boldsymbol{B}^{t+\Delta t} - \boldsymbol{B}^t}{\Delta t}\right] = -\nabla\times\boldsymbol{E}^t + \tau c^2 \Delta t \nabla^2 \boldsymbol{B}^t + \tau\frac{\Delta t}{\epsilon_0}\nabla\times\boldsymbol{J}^{t+\frac{\Delta t}{2}}. \tag{34}
$$

Eq. (34) can be solved with either spectral or iterative methods, since Eq. (34) is a second-order partial differential equation. In the present study, we first compute magnetic field $\boldsymbol{B}^{t+\Delta t}$ using the conjugate gradient method (e.g., [16]), and then update electric field $\boldsymbol{E}^{t+\Delta t}$ based on Eq. (32).

3. GEM reconnection setup

The initial condition is based on the Harris sheet equilibrium [17] in the x–y plane,

$$
B_x^{t=0}(y) = -B_0 \tanh\left(\frac{y}{\lambda}\right), \tag{35}
$$

where λ is the half thickness of the current sheet. Let us assume that the initial electrons and ions have a shifted Maxwellian distribution

$$f_s(\boldsymbol{x},\boldsymbol{v}) = n(y)\cdot\frac{1}{[\sqrt{2\pi}V_{ts}]^3}\exp\left(\frac{v_x^2+v_y^2+[v_z-V_{ds}]^2}{2V_{ts}^2}\right). \tag{36}$$

Then, the density distribution is given by

$$n^{t=0}(y) = \frac{n_0}{\cosh^2\left(\frac{y}{\lambda}\right)}, \tag{37}$$

where

$$n_0 = \frac{B_0}{q\mu_0[V_{di}-V_{de}]\lambda}. \tag{38}$$

Inserting Eq. (36) and (35) into Eq. (2) with $\frac{\partial}{\partial t}=0$, we obtain

$$\begin{aligned} V_{di} &= \frac{2m_iV_{ti}}{q_iB_0\lambda}, \\ V_{de} &= -\frac{2m_eV_{te}}{q_eB_0\lambda}. \end{aligned} \tag{39}$$

Thus the magnitude of magnetic field is written as

$$B_0 = \frac{\sqrt{2\left[\frac{m_i^2}{q_i^2}\omega_{pi}^2V_{ti}^2+\frac{m_e^2}{q_e^2}\omega_{pe}^2V_{te}^2\right]}}{c}. \tag{40}$$

The simulation setup is identical to the GEM magnetic reconnection challenge studies [1,2,6,18–20]. The total GEM system size is $L_x=\pm12.8\lambda_i$ in the x direction and $L_y=\pm6.4\lambda_i$ in the y direction, where λ_i is the ion inertial length $\lambda_i=c/\omega_{pi}$. The sheet half thickness is chosen to be $\lambda=0.5\lambda_i$. The temperature ratio is $T_i/T_e=5$ and a reduced mass ratio of $m_i/m_e=25$ is used. In addition a uniform background density $n_b=0.2n_0$ with the same temperature $T_{i,e}$ but without a drift velocity $V_{di,e}=0$ is included. An initial perturbation is also added to the magnetic vector potential component A_z with $\psi_0=0.1B_0\lambda_i$,

$$\psi(x,y) = \phi_0\cos\left[\frac{\pi}{L_x}x\right]\sin\left[\frac{\pi}{2L_y}y\right]. \tag{41}$$

To normalize the physical quantities, we choose $\omega_{pe}=1$ and $V_{te}=1$. Thus the electron Debye length becomes $\lambda_{De}=V_{te}/\omega_{pe}=1$. We also choose $\omega_{ce}/\omega_{pe}=0.25$. Thus the light speed and the Alfven speed become $c/V_{te}=13.86$ and $V_A/V_{te}=0.69$, respectively ($c/V_A=20$). The drift velocities are obtained as $V_{di}/V_{te}=1.15$ and $V_{de}/V_{te}=-0.23$. The ion inertial length becomes $\lambda_i/\lambda_e=69.28$. These parameters are identical to the PIC simulation by Pritchett [20].

Because of the symmetry constraints, we adopt the one quarter model which is common with Schmitz and Grauer [6]. We simulate only $0\leqslant x\leqslant L_x$ and $0\leqslant y\leqslant L_y$ with the symmetric boundary condition on $x=0$, L_x and $y=0$. The conducting wall is assumed on $y=L_y$.

In the velocity space, we solve $-8<v_e/V_{te}<8$ for electrons and $-4<v_i/V_{te}<4$ for ions in the cubic grid system ($\Delta v\equiv\Delta v_x=\Delta v_y=\Delta v_z$). The resolution in the velocity space is chosen to be $\Delta v=0.53V_{te}$ for electrons and $\Delta v=0.27V_{te}=0.6V_{ti}$ for ions, with $30\times30\times30$ grid points.

In the present full-electromagnetic Vlasov code, we have three CFL conditions. The first is the CFL condition for advection in configuration space,

$$\frac{1}{\sqrt{1/\Delta x^2+1/\Delta y^2}} > |\boldsymbol{v}_{\max}|\Delta t \tag{42}$$

which might not be important. The second is the CFL condition for advection in velocity space by electric fields,

$$\frac{1}{\sqrt{1/\Delta v_x^2+1/\Delta v_y^2+1/\Delta v_z^2}} > \frac{q}{m}|\boldsymbol{E}|\Delta t. \tag{43}$$

This becomes critical when there arises a strong electric field. The third is the CFL condition for rotation in velocity space by magnetic fields,

$$\frac{1}{\sqrt{1/\Delta v_x^2+1/\Delta v_y^2+1/\Delta v_z^2}} > \frac{q}{m}|\boldsymbol{v}_{\max}||\boldsymbol{B}|\Delta t \tag{44}$$

which is most important in the present study. For stable rotation of distribution functions on the Cartesian grid system, we choose $\omega_{pe}\Delta t=0.2$ that satisfies

$$\Delta v_e > \frac{q_e}{m_e}|\boldsymbol{v}_{\max,e}|B_0\Delta t = \omega_{ce}|\boldsymbol{v}_{\max,e}|\Delta t. \tag{45}$$

In the present study, we vary the grid spacing Δx ($=\Delta y$) and number of grid points in the x and y directions. The detailed parameters are listed in Table 1.

Table 1
Simulation parameters for different runs.

Run#	$N_x \times N_y$	$\Delta x = \Delta y$	Memory
1	256×128	$0.05\lambda_i = 3.46\lambda_{De}$	20 GB
2	128×64	$0.1\lambda_i = 6.93\lambda_{De}$	5 GB
3	64×32	$0.2\lambda_i = 13.86\lambda_{De}$	1.2 GB
4	32×16	$0.4\lambda_i = 27.71\lambda_{De}$	300 MB

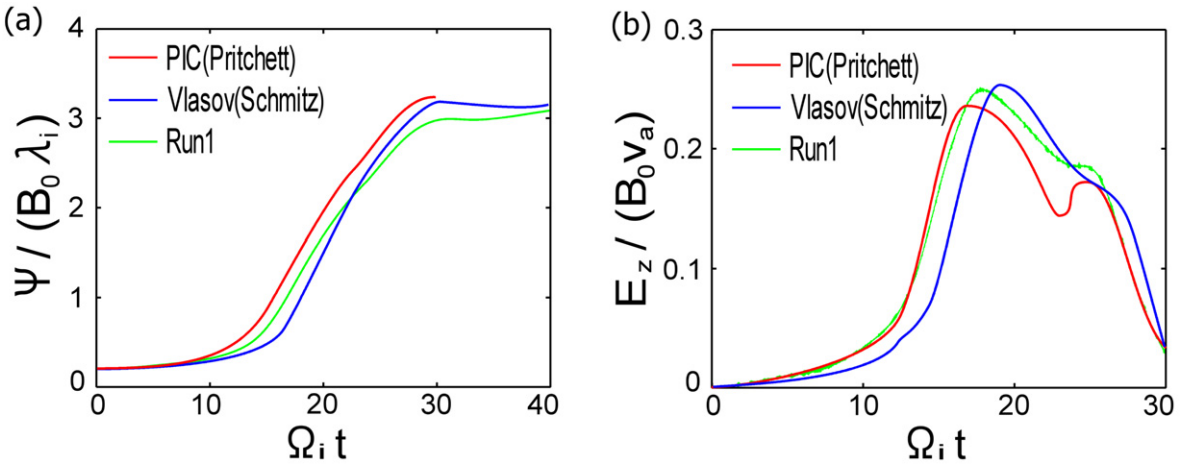

Fig. 2. Reconnected flux (a) and reconnection rate (b) as a function of time. The reconnected flux and the reconnection rate obtained with the full-EM Vlasov code are compared with the results with full-EM PIC code [20] and Darwin Vlasov code [6].

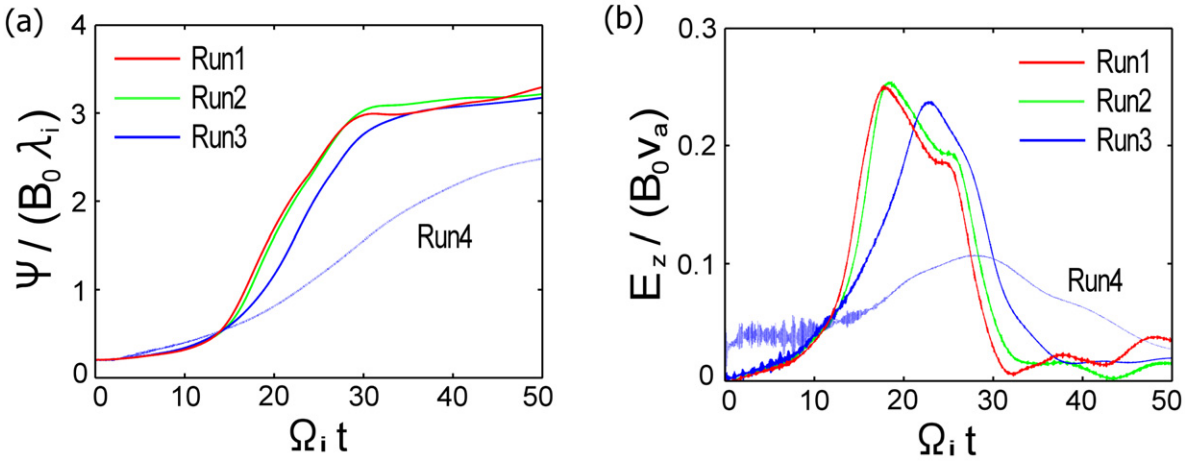

Fig. 3. Reconnected flux (a) and reconnection rate (b) as a function of time for Runs 1–4.

4. Results

As a measure of the reconnected magnetic field we use the difference of the magnetic vector potential component A_z between the X point and the O point,

$$\psi = \int_0^{L_x} B_y(x, y = 0)\,\mathrm{d}x = A_z(L_x, 0) - A_z(0, 0). \tag{46}$$

The reconnection rate is measured by the out-of-plane electric field at the X point.

$$\frac{\partial \psi}{\partial t} \simeq E_z(0, 0). \tag{47}$$

The time evolution of the reconnected flux and the reconnection rate in Run 1 is plotted in Fig. 2 and compared with the results with full-electromagnetic PIC code by Pritchett [20] and Darwin Vlasov code by Schmitz and Grauer [6]. The present result is in remarkable agreement with the previous kinetic simulations of the GEM reconnection challenge, suggesting that the unsplitting conservative scheme presented in this paper is useful to solve the Vlasov–Maxwell system equations with the charge conservation. Fig. 3 shows the time evolution of the reconnected flux and the reconnection rate obtained in four different runs 1–4. We found that the onsets of the fast reconnection are delayed as the spatial resolution becomes lower. In Runs 1–3, the time evolution of the reconnected flux is in agreement

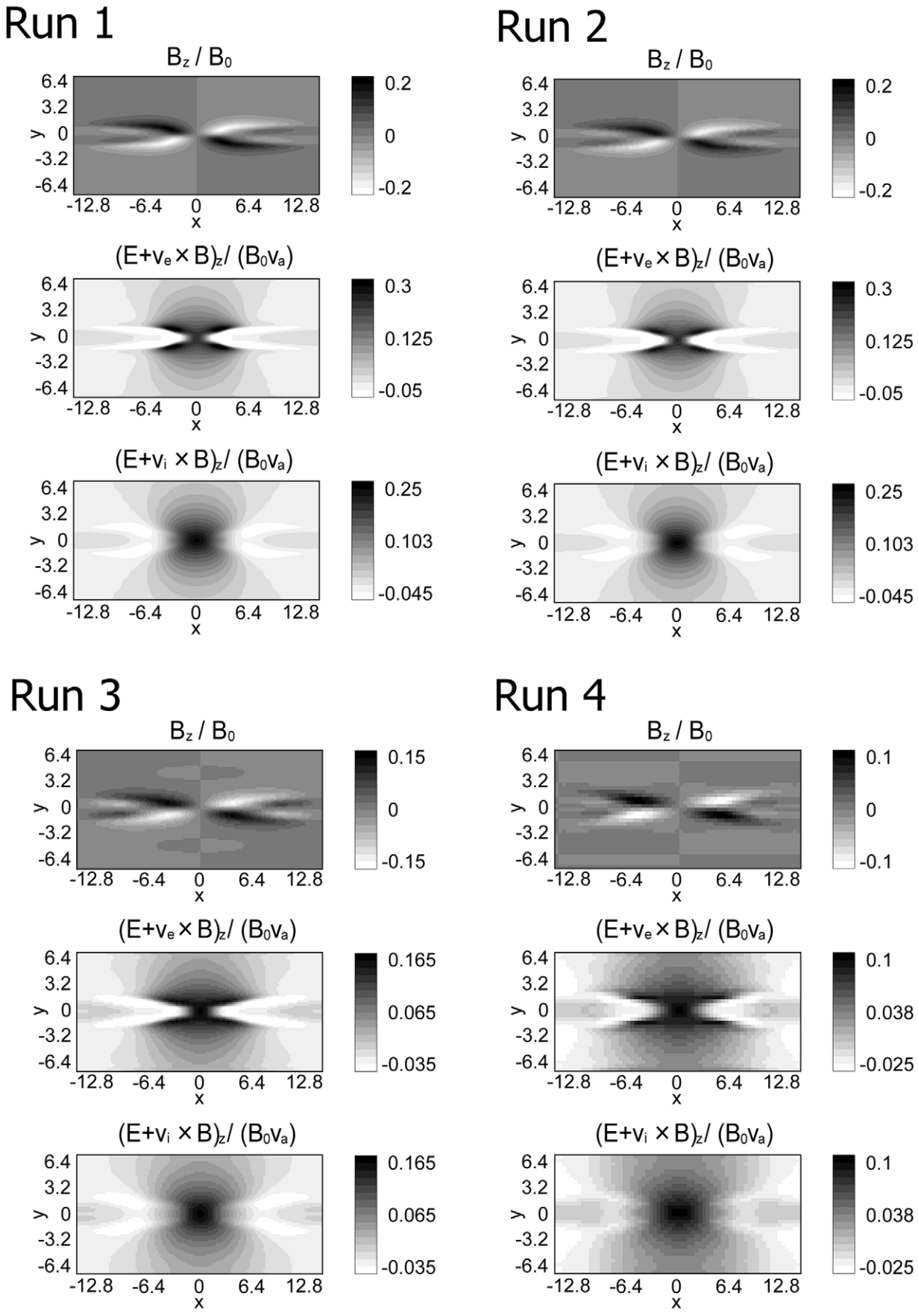

Fig. 4. Snapshots of out-of-plane magnetic field B_z, z components of $\boldsymbol{E} + \boldsymbol{v}_e \times \boldsymbol{B}$ and $\boldsymbol{E} + \boldsymbol{v}_i \times \boldsymbol{B}$ for Runs 1–4 when the reconnected flux reaches $\psi = B_0 \lambda_i$.

with the GEM reconnection challenge, while in Run 4 the reconnection evolves much slower than in other high-resolution runs. We found the fast reconnection ($E_z > 0.1$) in Runs 1–3. In contrast, the reconnection rate in Run 4 marginally exceeds $E_z = 0.1$, but the reconnection rate is much lower than that in other high-resolution runs. The time history of the reconnection rate in Run 4 shows some numerical oscillations likely due to error of numerical Harris equilibrium arising from the low resolution. We expect that $\Delta x = 0.4\lambda_i$ might be a threshold for fast magnetic reconnection in the present full-electromagnetic Vlasov code.

Fig. 4 shows out-of-plane magnetic field B_z, z components of $\boldsymbol{E} + \boldsymbol{v}_e \times \boldsymbol{B}$ and $\boldsymbol{E} + \boldsymbol{v}_i \times \boldsymbol{B}$ for Runs 1–4. We plot snapshots of these quantities when the reconnected flux reaches $\psi = B_0\lambda_i$. We can clearly identify the quadrupolar structure of out-of-plane magnetic field generated by the Hall currents [21]. In Runs 1 and 2, the magnitude of quadrupolar structure is the same, while in Runs 3 and 4 the magnitude becomes lower as the spatial resolution becomes lower. We also found that z component of $\boldsymbol{E} + \boldsymbol{v}_e \times \boldsymbol{B}$ and $\boldsymbol{E} + \boldsymbol{v}_i \times \boldsymbol{B}$ shows the same structure for Runs 1–4. The magnitude becomes lower as the spatial resolution becomes lower, but the magnitude is the same in Runs 1 and 2. These results suggest that the spatial resolution $\Delta x < 0.1\lambda_i$ is sufficient for fast reconnection. In the linear dispersion relation of low-frequency electromagnetic plasma waves, separation between R-mode whistler waves and L-mode ion cyclotron waves is identified at a wavenumber $k\lambda_i \sim 0.5$ (which corresponds to $\omega = kV_A \sim 0.5\omega_{ci}$). Thus the Hall effect is numerically suppressed when $\Delta x \geqslant 0.4\lambda_i$.

5. Summary

A full-electromagnetic Vlasov code has been presented. The code uses a positive, non-oscillatory and conservative scheme that can exactly satisfies the continuity equation for charge. An implicit FDTD method is also adopted for solving full-set of Maxwell's equations. Thus the time-integration of the Vlasov equation is restricted only by the CFL condition of cyclotron motion.

Then, simulations of GEM magnetic reconnection challenge have been performed to benchmark the full Maxwell–Vlasov system. The spatial grid spacing is taken to be much larger than the electron Debye length. It is also found that Hall effect is numerically suppressed when the spatial resolution is lower $\Delta x \geqslant 0.4\lambda_i$. The spatial resolution $\Delta x < 0.1\lambda_i$ is sufficient for fast reconnection. It has been also shown that the Vlasov simulation is free from the numerical instability caused by the resolution in configuration space relative to the Debye length. This is an advantage over the explicit PIC method. Thus full-electromagnetic Vlasov code presented here might be useful for full-kinetic simulation of large-scale processes in plasmas.

Acknowledgements

We thank Keizo Fujimoto for discussions. This work was supported by Grant-in-Aid for Young Scientists (Start-up) #19840024 from Japan Society for the Promotion of Science and in part by Grant-in-Aid for Creative Scientific Research #17GS0208 "The Basic Study of Space Weather Prediction" from the Ministry of Education, Science, Sports, Technology, and Culture of Japan. The computer simulations were performed on the Fujitsu PRIMEPOWER HPC2500 at Information Technology Center, Nagoya University as a collaborative computational research project at Solar-Terrestrial Environment Laboratory, Nagoya University.

References

[1] J. Birn, J.F. Drake, M.A. Shay, B.N. Rogers, R.E. Denton, M. Hesse, M. Kuznetsova, Z.W. Ma, A. Bhattacharjee, A. Otto, P.L. Pritchett, Geospace Environmental Modeling (GEM) magnetic reconnection challenge, J. Geophys. Res. 106 (2001) 3715–3719.
[2] P. Ricci, G. Lapenta, J.U. Brackbill, GEM reconnection challenge: Implicit kinetic simulations with the physical mass ratio, Geophys. Res. Lett. 29 (2002) 2088–2091.
[3] K. Fujimoto, R.D. Sydora, Electromagnetic particle-in-cell simulations on magnetic reconnection with adaptive mesh refinement, Comput. Phys. Comm. 178 (2008) 915–923.
[4] M.R. Gibbons, D.W. Hewett, The Darwin direct implicit particle-in-cell method for simulation of low frequency plasma phenomena, J. Comput. Phys. 120 (1995) 231–247.
[5] H. Schmitz, R. Grauer, Darwin–Vlasov simulations of magnetised plasmas, J. Comput. Phys. 214 (2006) 738–756.
[6] H. Schmitz, R. Grauer, Kinetic Vlasov simulations of collisionless magnetic reconnection, Phys. Plasmas 13 (2006) 092309.
[7] C.Z. Cheng, G. Knorr, The integration of the Vlasov equation in configuration space, J. Comput. Phys. 22 (1976) 330–351.
[8] C.Z. Cheng, The integration of the Vlasov equation for a magnetized plasma, J. Comput. Phys. 24 (1977) 348–360.
[9] A. Ghizzo, F. Huot, P. Bertrand, A non-periodic 2D semi-Lagrangian Vlasov code for laser-plasma interaction on parallel computer, J. Comput. Phys. 186 (2003) 47–69.
[10] H. Schmitz, R. Grauer, Comparison of time splitting and backsubstitution methods for integrating Vlasov's equation with magnetic fields, Comput. Phys. Comm. 175 (2006) 86–92.
[11] N.V. Elkina, J. Buchner, A new conservative unsplit method for the solution of the Vlasov equation, J. Comput. Phys. 213 (2005) 862–875.
[12] T. Umeda, A conservative and non-oscillatory scheme for Vlasov code simulations, Earth Planets Space 60 (2008) 773–779.
[13] F. Filbet, E. Sonnendrucker, P. Bertrand, Conservative numerical schemes for the Vlasov equation, J. Comput. Phys. 172 (2001) 166–187.
[14] T. Umeda, M. Ashour-Abdalla, D. Schriver, Comparison of numerical interpolation schemes for one-dimensional electrostatic Vlasov code, J. Plasma Phys. 72 (2006) 1057–1060.
[15] K.S. Yee, Numerical solution of initial boundary value problems involving Maxwell's equations in isotropic media, IEEE Trans. Antenn. Propagat. AP-14 (1966) 302–307.
[16] M. Hoshino, Theoretical and computational studies of plasma kinetic phenomena: Tearing mode instability and foreshock cyclotron interaction, PhD Thesis, University of Tokyo, Tokyo, 1986.
[17] E.G. Harris, On a plasma sheath separating regions of oppositely directed magnetic field, Nuovo Cimento 23 (1962) 115–121.
[18] J. Birn, M. Hesse, Geospace Environment Modeling (GEM) magnetic reconnection challenge: Resistive tearing, anisotropic pressure and Hall effects, J. Geophys. Res. 106 (2001) 3737–3750.
[19] M. Hesse, J. Birn, M. Kuznetsova, Collisionless magnetic reconnection: Electron processes and transport modeling, J. Geophys. Res. 106 (2001) 3721–3735.
[20] P.L. Pritchett, Geospace Environment Modeling magnetic reconnection challenge: Simulations with a full particle electromagnetic code, J. Geophys. Res. 106 (2001) 3783–3798.
[21] T. Terasawa, Hall current effect on tearing mode instability, Geophys. Res. Lett. 10 (1986) 475–478.